International Journal of Physical Sciences

Volume 9 Number 13 16 July, 2014

ISSN 1992-1950

Academic Journals

ABOUT IJPS

The **International Journal of Physical Sciences (IJPS)** is published weekly (one volume per year) by Academic Journals.

International Journal of Physical Sciences (IJPS) is an open access journal that publishes high-quality solicited and unsolicited articles, in English, in all Physics and chemistry including artificial intelligence, neural processing, nuclear and particle physics, geophysics, physics in medicine and biology, plasma physics, semiconductor science and technology, wireless and optical communications, materials science, energy and fuels, environmental science and technology, combinatorial chemistry, natural products, molecular therapeutics, geochemistry, cement and concrete research, metallurgy, crystallography and computer-aided materials design. All articles published in IJPS are peer-reviewed.

Contact Us

Editorial Office: ijps@academicjournals.org

Help Desk: helpdesk@academicjournals.org

Website: http://www.academicjournals.org/journal/IJPS

Submit manuscript online http://ms.academicjournals.me/

Editorial Board

International Journal of Physical Sciences

Table of Contents: Volume 9 Number 13, 16 July, 2014

ARTICLES

academicJournals

Vol. Vol. 9(13), pp. 292-301, 16 July, 2014
DOI: 10.5897/IJPS2014.4147
ISSN 1992 - 1950
Article Number: 56C1A3D46333

http://www.academicjournals.org/IJPS

International Journal of Physical Sciences

Full Length Research Paper

Optical observation of streamer propagation and breakdown in seed based insulating oil under impulse voltages

Essam A. Al-Ammar

Saudi Aramco Chair in Electrical Power, Department of Electrical Engineering, King Saud University, Riyadh, Saudi Arabia.

Received 16 March, 2014; Accepted 10 July, 2014

Increasing demand of electricity and high consumption of natural fuel resources has raised countless challenges for the electricity industry. For years, transformers were equipped with mineral oil for better and lasting performance but the recent uncertainty about the future of oil availability is motivating the researchers to find out the "Green Insulating Oils" for transformers. Thus, green insulating oils are being probed with great interest at research centers worldwide. In this paper, Canola oil was studied for applications in transformers as a sustainable solution. The paper also compared the proposed oil with mineral oil by studying the initiation and propagation of streamers in the oils when subjected to standard lightning impulse voltages. It also presents experimental results of a comparative study of initiation and propagation of streamers in canola seed based oil and mineral insulating oil when subjected under standard lightning impulse voltages. Moreover, streamer patterns, modes of propagation and their stopping lengths were investigated under both polarities of voltage in point-plane electrode gap. The paper concludes with six different findings, which states that canola oil is a better and sustainable choice of oil for transformer use.

Key words: Breakdown, impulse voltage, oil, seed based insulating oil, streamer propagation.

INTRODUCTION

Mineral oil based dielectric fluids are applied in a large variety of electrical power equipment. Worldwide estimates show that almost 30 to 40 million tons of mineral insulating oils are in use. The functions of these oils are to fill the air cavities of the porous solid insulation in order to improve its partial discharge behavior as well as to act as a heat transfer medium to dissipate the losses (Oommen, 2002). However, mineral oils are easily flammable, are poorly degradable and can contaminate soil and water, if spillover takes place. In addition, the increasing crisis of petroleum oil that is currently leading to uncertainty in its sustainable supply has forced the researchers worldwide to find suitable alternate sources (Claiborne et al., 1999; Amanullah et al., 2005; Perrier et al., 2004).

In this context, the vegetable seed oils are natural

E-mail: essam@ksu.edu.sa

Table 1. Measured properties of the investigated fluids.

Property		Unit	Canola Oil	Mineral Oil
Density at 23°C		kg/dm^3	0.98	0.89
Viscosity at:	30°C	Mm^2 /s	28	23
	60°C		12	6.5
Acidity		mg/KOH/g	0.1315	0.056
Water Content		ppm	125	15
(60 Hz) AC Breakdown Voltage using IEC Mushroom Electrodes with 1.0 mm separation		kVrms	43	34
Dielectric Dissipation Factor (tan δ)	23°C		0.0027	0.0011
	80°C		0.019	0.01
Permittivity (ε_r) at	23°C		3.07	2.2
	80°C		2.85	2.05

products and have renewable sources with plenty of supply and present suitable “green products” that can replace the mineral based oils. Their most attractive features are the high biodegradability (95 to 100%) and higher fire point (~360°C) instead of ~160°C for most mineral based insulating oils. Researches on pre-breakdown and breakdown phenomena of mineral based insulating liquids have been progressing since 1950s (Sharbaugh et al., 1978; Beroual et al., 1998) respectively. Martin and Wang (2008); Rapp et al. (2009) and Yasuda et al. (2010) exemplify the use of vegetable oils for dielectric applications in power distribution transformers and other high voltage equipments. Nevertheless, recently transformer-grade vegetable oils are also commercially available. The first commercial product was BIOTEMP, patented in the U.S. in September 1999 by ABB. Another U.S. patent was also issued in September 1999 for transformer oil which uses regular soybean oil. Moreover, another U.S. patent was granted to Cooper Industries, Inc. under the trademark of Envirotemp FR3 (Moumine et al., 1995).

This fluid is based on standard-grade oleic oils, and is used commercially in some distribution transformers. Subsequent patents were also issued to the ABB inventors on the BIOTEMP fluid in August 2001 (Oommen and Claiborne, 1999; McShane et al., 2000).

In Badent et al. (2000) two types of oils that is, Vegetable Canola oil (VO) and Transformer grade mineral oil (MO) are investigated. Canola oil is kitchen grade pure oil and its main molecular composition is triglycerides and fatty acid containing both saturated as well unsaturated fatty components with up to 23 carbon chain lengths containing double bonds. Due to the presence of double bonds, it is prone to oxidation under thermal stress when in contact with copper or other metals. To overcome these problems, antioxidants such as Butylated Hydroxyanisole (BHA) and Butylated Hydroxytoluene are mixed in the bulk oil. Moreover, further reason to select the Canola oil is that several ester groups and other radicals are also present in Canola oil. The viscosity neutralization number and dissipation factor in Canola oil are higher than in mineral oil but these are within the accepted limits specified in international standards for mineral insulating oils. The higher values of permittivity at ε_r = 3.07 and hydrophilic character of Canola oil is expected to provide better edge to designers as compared to mineral oil, provided it is chemically synthesized and refined by stripping it off the radicals that make it prone toward oxidation and the ones that control its viscosity.

On the other hand, mineral oil molecules mainly consist of carbon and hydrogen atoms arranged in different structures such as paraffinic, naphthenic and aromatics. Their composition varies depending on the source, and the aromatic content plays a major role in the formulation of the streamer shapes (Badent et al., 2000; Devins et al., 1981). Some salient properties of these oils were measured in the laboratory and are summarized in Table 1.

EXPERIMENTAL SETUP

The experiment set up for detection of initiation and propagation of streamers in the investigated liquids is shown in Figure 1. A test cell comprising of point-plane electrode system was designed and used. Its main body was made of PTFE material and its top lid was of transparent PMMA (”Perspex”) to facilitate the observation of inter electrode gap events. Tungsten and high carbon steel needles with tip radius (r_p) of 10 µm were used. The plane electrode was made of brass having a diameter of 50 mm with its edges rounded.

A Perspex sheet barrier of 3 mm thickness was embedded on its surface to protect the electrode and the attached detection equipment at the advent of oil breakdowns. The electrode gap was arranged in horizontal format and is shown in Figure 2. Haefely 10-

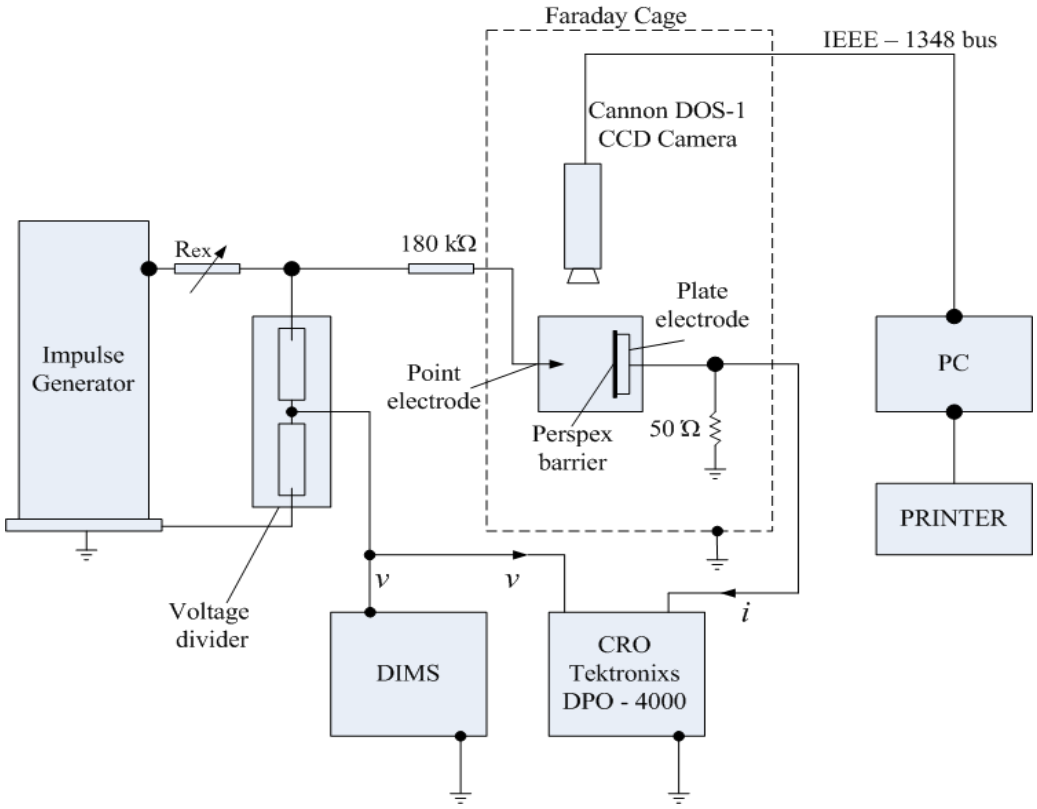

Figure 1. Sketch of experimental set up.

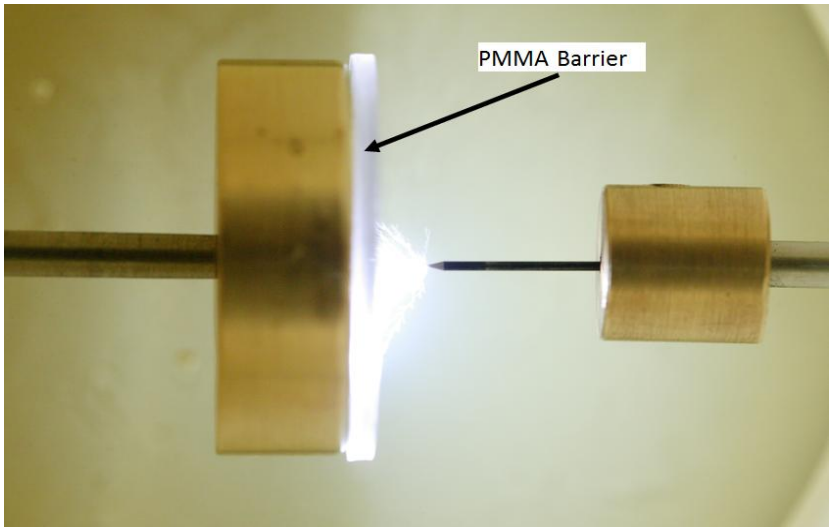

Figure 2. Electrode gap in the test cell.

stage impulse generator with 100 kV, 4 kJ output per stage was used to produce standard lightning impulse voltages which were measured through an RC voltage divider and Digital Impulse Measuring System (DIMS). The voltage signal and current signal coming from the precision non-inductive 50 Ω resistor were fed to a 400 MHz oscilloscope for data acquisition. A 180 kΩ resistor was connected at the output of the impulse generator to limit the breakdown current and injected energy into the test cell.

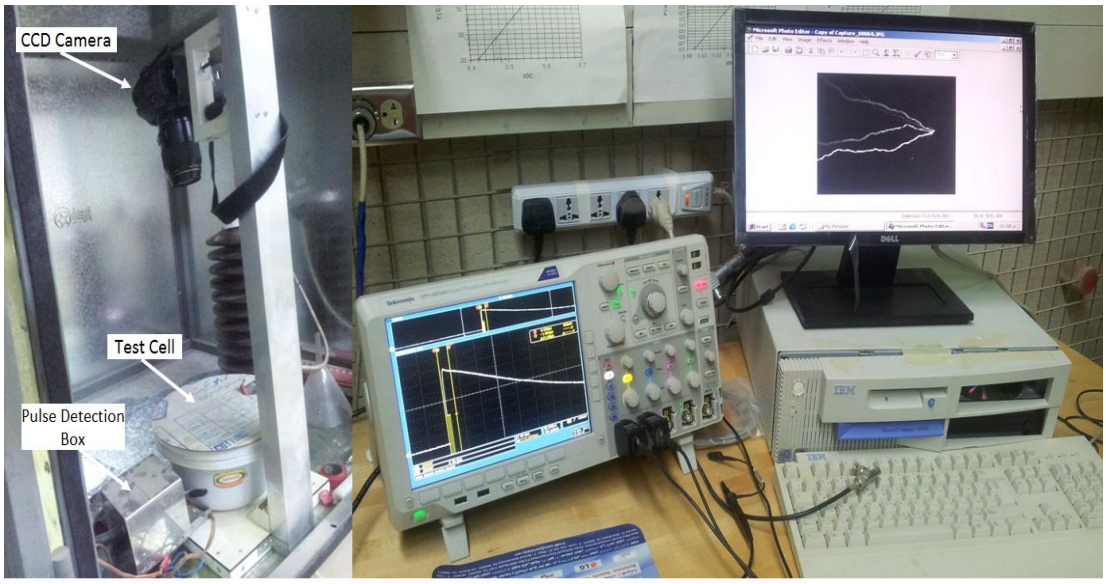

Figure 3. Experimental arrangement: (a) CCD camera, test cell and pulse detection box, (b) PC and oscilloscope connected with the incoming signal cables.

The shadowgraph system consisting of a 15 Mega pixel CCD Camera, which could be used with or without a flash was employed. Instead of conventional shadow graphic system in which the streamer channels are displayed in the background of a trigger light pulse, the self-irradiated light from filaments of streamers was used to capture the events. The camera was opened for 5 s synchronously with the operation of the trigger pulse applied to the impulse generator. This exposure time and any delay in the operation of trigger system were found optimum to capture the events associated with the applied voltage impulse. Moreover, Figure 3 displays photographically the set up with camera, test cell and other detection instruments connected together.

RESULTS AND DISCUSSION

Streamer characteristics of the two types of oils mentioned earlier were investigated. Comparisons were made for the shapes using propagation modes including their stopping lengths. This study was mostly carried out using a middle size electrode gap of 20 mm (from industrial application's point of view), with a point electrode tip of 10 µm radius. The streamer shapes in mineral oils had the same behavior as had already been reported in (Dang et al., 2012) and therefore these were not documented here to avoid duplication. Therefore, results presented here are for the streamers in Canola oil that were captured using both polarities of standard lightning impulse voltages (1.2/50 µs). However, the analysis and discussion are made for both types of the oils investigated that is mineral oil and canola oil.

Electrical characteristics of selected oils

The most important properties of insulating oils are the dielectric ones beside the usual physico-chemical characteristics. Vegetable oils possess high flash and fire point as compared to mineral based oil. This typical character lends strong support to adopt these oils in transformers located in hazardous locations. The combination of fire safety and high biodegradability (> 98%) can eliminate the traditional need for fire walls and deludge systems built around transformer banks (McShane et al., 1999; CIGRE WG A2-35 Brochure, 2010).

The A.C breakdown strength of vegetable oils was not affected with moisture intake up to 300 ppm, where as the moisture present in mineral oil (MO) has very deleterious impact on its properties (CIGRE WG A2-35 Brochure, 2010).The use of vegetable oil in combination with cellulose in transformer helps in drying out the later as it absorbs its moisture when in contact (Martin, 2010). Several groups of investigators (Perrier et al., 2004; Beroual et al., 1998; Rapp et al., 2009; Dang et al., 2012) have reported higher power frequency breakdown strength of conola oil as compared to mineral oil.

On the other hand, a number of studies on traditional mineral oil were published (Lesaint and Massala, 1998; Massala and Lesaint, 2001; Linhjell et al., 1994; Torshin, 2003, 2009; Lopatin et al., 1998) describing the streamer initiation and propagation in terms of velocity and shape, streamer mechanism and streamer modeling.

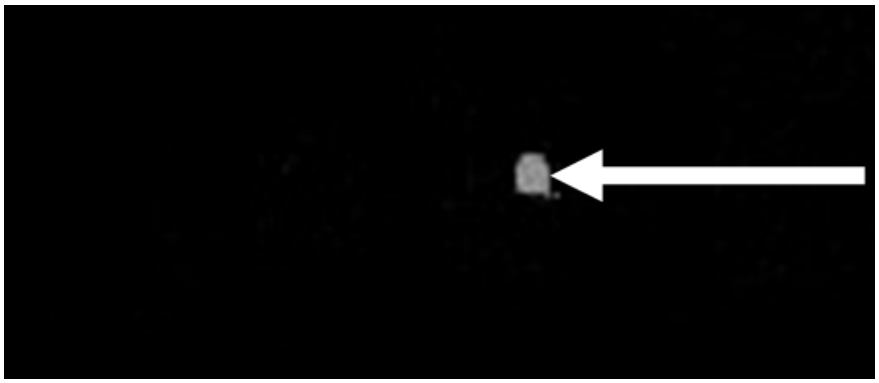

Figure 4. Streamer onset in Canola oil under negative lightening impulse voltage.

It is acknowledged that impulse pre-breakdown and breakdown characteristics are related to chemical composition of the liquid, so application of esters (with composition different to mineral oil) calls for detailed investigation under impulse voltage. Some papers on this topic were reported in Badent et al. (2000) and Duy et al. (2009). Streamer stopping length, propagation velocity, 50% breakdown voltage and acceleration voltage of natural ester (rape-seed oil) were also documented, which showed easier propagation of streamers in ester and consequently lower breakdown voltage than mineral oil. Hestac et al. (2004) reported the streamer inception voltages of rape-seed oil at 8 and 20 mm tip-plane gaps, were about 50% lower than that of mineral oil. Streamer initiation in a synthetic ester (Midel 7131) under strong non-uniform field was studied in Viet-Hung et al. (2012) which was found to be about 60% higher than that of mineral oil.

Streamer patterns in canola oil

Negative polarity streamer

At first the approximate breakdown level of the oil gap was determined and then starting from around 70% of this voltage level, the applied voltage three consecutive shots were applied at each set level. If no event was observed, the voltage was increased in steps of 2 kV_p. The streamer initiation voltage (V_i) was registered if it appeared under all three applied shots. At the onset, a faint minuscule light appears in the vicinity of the point electrode as shown in Figure 4a. With an increase in voltage, it expanded with instabilities appearing on its surface as shown in Figure 5b. One or two of the instabilities enlarged with increase in voltage and propagated toward the plane electrode. As the streamers increased in size, more filaments appeared as off-shoots from these enlarged filaments as shown in a sequence of events captured independently at different intervals as shown in Figure 5b-g. Figure 5g displays the breakdown event as captured at well above the breakdown voltage level which it impinged on the plane electrode.

It is clear that as the voltage is increased, more number of luminous branches appears and was propagated towards the plane electrode. The first one which came in contact with the plane electrode caused a flow of large current leading to the formation of a plasma channel which emanates strong light intensity light. This channel was also clearly seen in this image. Since the picture captured was in 2-dimensions while the streamer pattern propagated in 3-dimensions the filaments that were closer to the observation system appeared brighter while the ones that were away from the observation point exhibited less luminosity. It is to be noted here that the streamer propagating in mineral oil were less branched and more luminous than observed in Canola oil.

Positive polarity streamer

It was more difficult to capture the initiation event of streamers under positive polarity lightning impulses. The reason is that the streamers once initiated, propagate very swiftly with long branches. Figure 6a exhibits a white spot which indicated initiation of a positive streamer. It was much brighter than the initial initiation spot that was observed in the vicinity under negative impulses point electrode. As soon as the voltage was increased to the next step, large size filaments appeared and propagated much faster compared to streamers under negative polarity. Figure 7c-f show propagated streamer shapes captured with increasing voltage.

In case of the positive streamer, a single large streamer with bright luminosity resulted in the breakdown of the gap as shown in Figure 7g and it was observed to exert a much stronger shock-wave than the corresponding

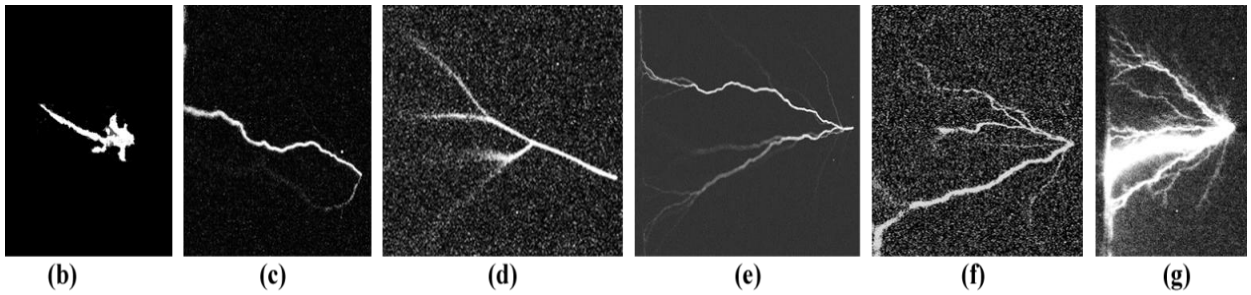

Figure 5. Sequence of initiation and propagation of negative streamers in vegetable oil. Electrode gap = 20 mm; Point tip radius = 10 µm (b) V = 65 kVp, (c) V = 73 kVp, (d) V = 75 kVp, (e) V = 85 kVp, (f) V = 90 kVp, (g) Breakdown event at -97 kVp.

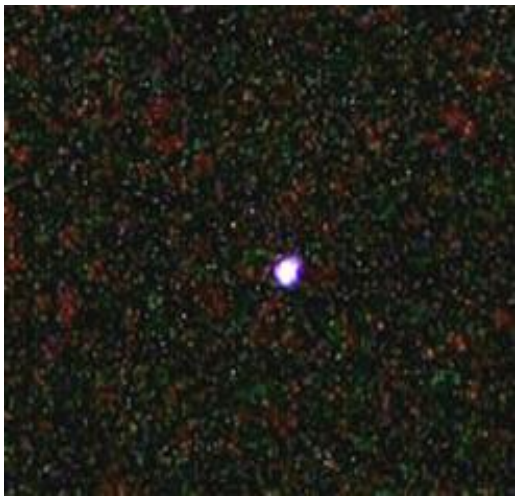

Figure 6. Positive streamer onset.

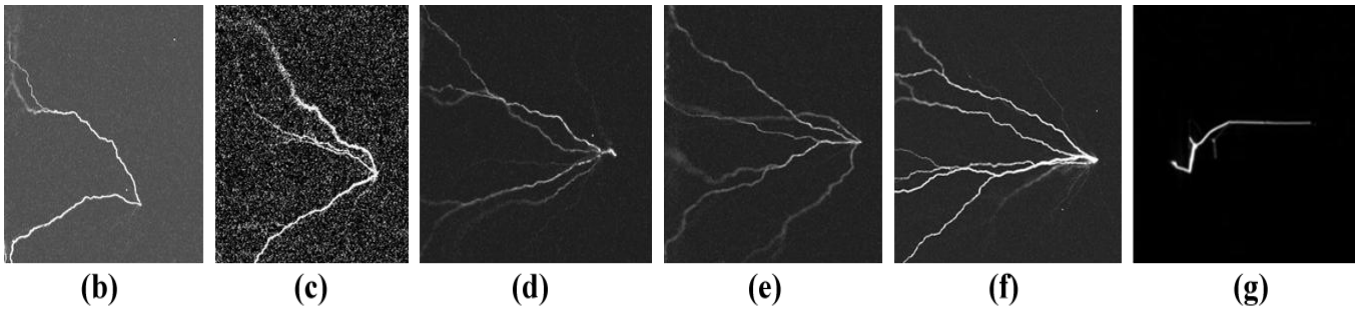

Figure 7. Sequence of initiation and propagation of positive streamers in vegetable oil. Electrode gap = 20 mm; point tip radius = 10 µm (b) V=57 kVp (c) V=62 kVp, (d) V=70 kVp, (e): V=81 kVp, (f): V=83 kVp, (g) Breakdown streamer at V=98 kVp.

negative streamer breakdown. It was also observed that the positive streamers, both in mineral oil as well as Canola oil were filamentary and less branched than the negative streamers.

Furthermore, in case of canola oil the streamers propagated to longer lengths and they were faster, especially once they cross the mid-gap spacing. These observations suggest that positive streamers in Canola

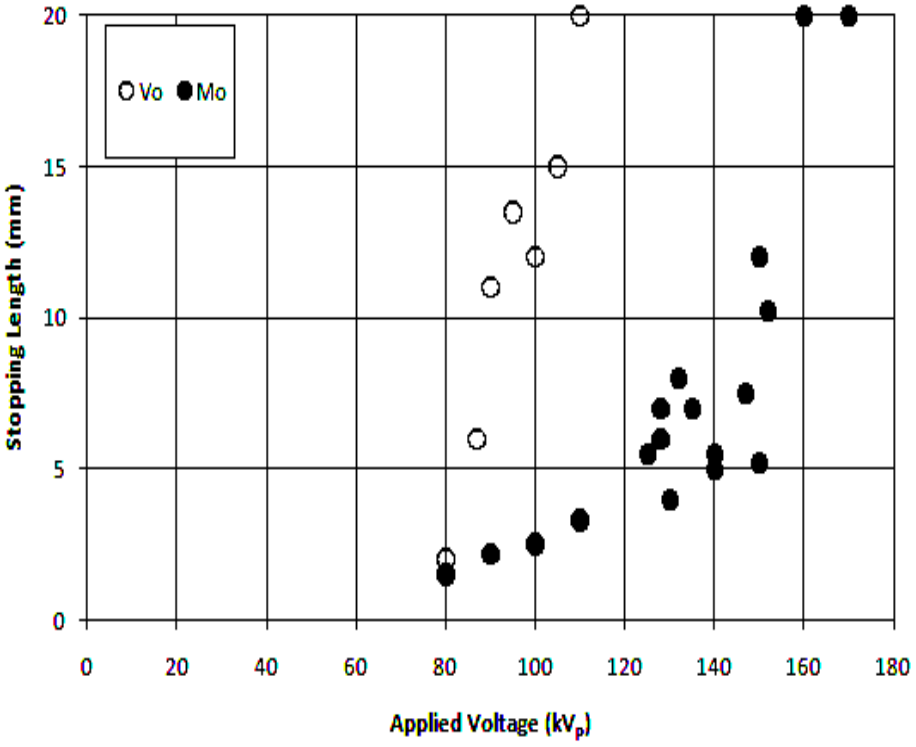

Figure 8. Final stopping lengths of negative streamers in Canola and mineral oils as a function of applied voltage. Gap spacing = 20 mm; point tip radius = 10 µm.

oil underwent different propagation modes as compared to these in mineral oil. However, this observation needs further experimental studies in order to isolate the occurrence of these differing modes and the shapes of associated streamers.

Stopping lengths of streamers

Figure 8 displays the comparison of final stopping lengths (L_f) of streamers under the application of preset voltage impulses of negative polarity lightning impulses for canola oil and mineral oil. These lengths were measured as the axial distance from the point electrode to the plane electrode. In case of mineral oil, the L_f increases almost linearly up to a voltage level of about 125 kV_p, where after, a large scatter was observed in the L_f values over the applied voltage range of 125 to 147 kV_p. Beyond this voltage level the L_f tends toward a very rapid rise up to breakdown voltage level of the gap. This was consistent with the results reported earlier by Dang et al. (2012) for mineral oil under similar gap configuration and by Liu et al. (2009) in 50 mm gap spacing. Moreover, from Figure 8, it was also observed that mineral oil had an exponential increase in applied voltage against the increase of stopping length.

This certainly explains that with the rise in voltage amplitude the negative streamer undergoes three different modes of propagation. The first mode in which the L_f propagates with lower velocity is generally confined to a gap range of about 0.3 d (where d = gap spacing). The second mode consists of medium velocity and displays large scatter in L_f values and occurs in the gap range of 0.3 to 0.5 d. Beyond the gap range of 0.5 d, the negative streamers propagate at much faster speed.

In Canola oil, too, the slower mode was confined in gap spacing of about 0.3 d. However, in this case, the second mode was not present, since the L_f values increased rapidly with further increase in the voltage. At a fixed voltage level, the L_f values in Canola oil were comparatively much longer than in mineral oil. This is why the negative polarity breakdown voltage of mineral oil was about 40% higher than in the Canola oil. This effect is opposite to AC breakdown voltage values reported in Table 1, where the AC breakdown voltage of Canola oil was almost 27% higher than in MO. However, its higher permittivity ($\varepsilon_r = 3.1$) which is comparable to transformer press board ($\varepsilon_r = 3.7$) and its typical hydrophilic character shall impose much beneficial effect

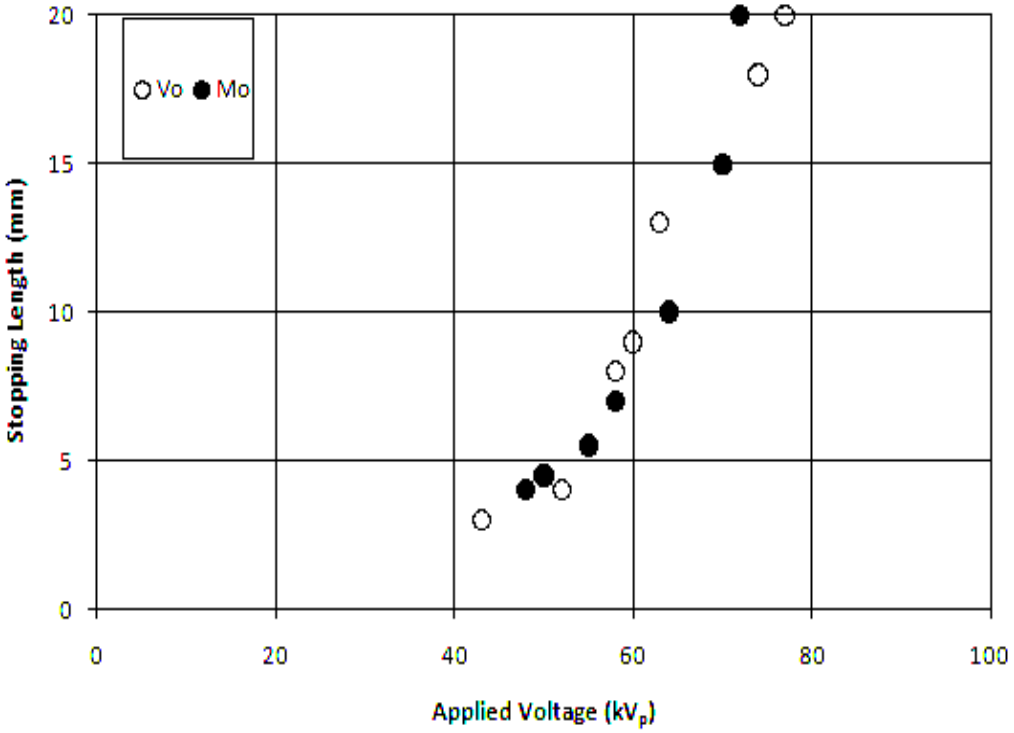

Figure 9. Final stopping lengths of positive streamers in Canola and mineral oils as a function of applied voltage. Gap spacing = 20 mm; point tip radius = 10 µm.

on the drying of cellulose and thus shall provide an offset toward its lower impulse breakdown strength. Therefore, by this experimental study, it could be concluded that Canola oil can be further refined to come at par with mineral insulating oil's properties and could be used as a good "Green Insulating Oil".

It has been reported earlier in their pioneer work by Devins et al. (1981) and later by others (Yasuda et al., 2010; Chadband and Sufian, 1985; Nelson, 1980; Kelley and Hebner, 1981) that the electron affinity of liquid molecules played a dominant role in the propagation of streamers. The molecule of Canola oil contains three esters (−C OOR) which have electro-negative oxygen atoms. These atoms may be the source behind swift propagation of negative streamers as well as for more branches that emanated from the initiated streamer trunk, as portrayed in Figure 5.

Figure 9 compared the L_f values of positive streamers as a function of applied voltage for both investigated oils. The streamer length versus transitions observed under negative polarity was not distinct under positive polarity. Moreover, the increase in L_f values with increase in the applied voltage was almost similar in both oils. Small scatter was noticed in L_f values but it was present in both oils. Moreover, it could also be observed that in positive streamer, both canola and mineral oil had a linear increase in applied voltage with respect to stopping length. The transition in this case occurred, around 56 kV_p. Under positive polarity lightning impulses, which streamers propagate very fast the streamers propagate much faster than under negative polarity, while their more luminous filaments indicated that they were more conducting than their negative counterparts. Whereas several negative streamer filaments impinge on plane electrode at the breakdown only one filament of the positive streamer that came in contact with the plane electrode became very luminous and caused a breakdown. Its stem remained initially bluish but this bluish color changed to bright white color in time as well as with the increase in the applied voltage. This aspect of positive streamer needs further investigations using a faster optical event capturing system.

As the negative or positive streamer propagates in the gap it traversed with certain velocity. Moreover, the voltage drop (ΔV) across the length of the streamer from the point electrode to the streamer head caused it to finally stop. Therefore, it depended on the local field at the point electrode as well as the mean electric field in the inter-electrode gap. The average field in the streamer could be evaluated from the 'L_f - V' characteristics of streamers in each oil and for each

polarity of the applied voltage. Thus, average longitudinal electric field 'E_l' within the streamer channel followed the relation $E_l = \Delta V/\Delta L_f$.The deduced value of E_l for positive streamers for both oils was about 1.6 MV/m, whereas it was about 2.0 MV/m for the faster mode and around 6 MV/m for the slower negative streamer's mode observed near the inception in the mineral oil. Interestingly, E_l value for faster mode of negative streamers in Canola oil approached close to that of positive streamer values. The lower E_l values indicated that these streamers were more conducting. It is a well known fact that the more conducting the streamer, the more rapid it propagated through the electrode gap (Beroual et al., 1998; Badent et al., 2000; Devins et al., 1981; Nelson, 1980).

Conclusions

This paper has reported on streamer initiation and their propagation in seed based Canola oil and mineral insulating oil used in transformers. This study leads to the following main conclusions:

1. Negative polarity streamers in Canola oil were more branched than in mineral oil.
2. Propagation of negative steamers in mineral oil exhibit three distinct modes, whereas only two modes were detected in canola oil.
3. The streamer stopping length in Canola oil for the same voltage was much longer than in mineral oil. This leads to lowering of the impulse breakdown strength of Canola oil as compared to the mineral oil.
4. The conductivity of positive streamers was higher than those of negative streamers in both oils, while the stopping lengths of those streamers were almost close to each other in both liquids.
5. Positive streamers were less branched than negative streamers.
6. The AC breakdown strength of Canola oil was 27% higher than mineral oil but it was 40% lower under lightning impulse voltage.

However, it is tough to explicitly declare that Canola oil is better than mineral oil. But from the given set of experiment and results, it has been found that canola oil has high potential to be used in transformers. These results also support a statement and new area of research that slight alteration in canola oil can produce significant effect over its properties and could be perfectly suitable for transformers.

Conflict of Interest

The author(s) have not declared any conflict of interest.

ACKNOWLEDGEMENTS

The author would like to thank Saudi Aramco Chair in Electrical Power for technical guidance and financial funding. Special gratitude is due to Prof. Abdulrahman Arainy, Prof. Nazar Malik, Prof. Abdhulrhaman Beroual, and Dr. Mohammed I. Qureshi for always being around and providing invaluable comments. The author also wishes to thank Engr. Muhammad Babar and Eng. Nissar Wani for their help in preparing the experimental setup.

REFERENCES

Amanullah M, Islam S, Chami S, Ienco G (2005). "Analyses of electro-chemical characteristics of vegetable oils as an alternative source to mineral oil-based dielectric fluid," in IEEE Int. Conf. Dielectric Liquids, 2005, pp. 397–400.

Badent R, Hemmer M, Konekamp U, Julliard Y, Schwab A (2000). "Streamer inception field strengths in rape-seed oils," in Annual Report Conference on Electrical Insulation and Dielectric Phenomena, 2000, vol. 1. IEEE, 2000, pp. 272–275.

Beroual A, Zahn M, Badent A, Kist K, Schwabe A, Yamashita H, Yamazawa K, Danikas M, Chadband W, Torshin Y (1998). "Propagation and structure of streamers in liquid dielectrics," IEEE Elect. Insul. Magazine 14(2):6–17.

Chadband W, Sufian T (1985). "Experimental support for a model of positive streamer propagation in liquid insulation," IEEE Trans. Electr. Insul. 2:239–246.

CIGRE WG A2-35 Brochure, No. 436, October 2010.

Claiborne C, Walsh E, Oommen T (1999). "An agriculturally based biodegradable dielectric fluid," in IEEE Trans. Distribution Conf. 2:876–881.

Dang V, Beroual A, Perrier C (2012). "Investigations on streamers phenomena in mineral, synthetic and natural ester oils under lightning impulse voltage," IEEE Trans. Dielectrics Elect. Insul. 19(5):1521–1527.

Devins J, Rzad S, Schwabe R (1981). "Breakdown and prebreakdown phenomena in liquids," J. Appl. Phys. 52(7):4531–4545.

Duy CT, Lesaint O, Denat A, Bonifaci N (2009). "Streamer Propagation and Breakdown in Natural Ester at High Voltage", IEEE Trans. Dielectrics Electr. Insul. 16(6):1582-1594.

Hestac OL, Berg G, Ingebrigtsen S, Lundgaard LE (2004). "Streamer Injection and Growth under Impulse Voltage: A Comparison of Cyclohexane, Midel 7131 and Nytro 10X", IEEE. Conf. Electr. Insul. Dielectrics Phenomena (CEIDP), Colorado, USA, pp. 542-546.

Kelley E, Hebner R (1981). "The electric field distribution associated with pre-breakdown phenomena in nitrobenzene," J. Appl. Phys. 52(1):191–195.

Lesaint O, Massala G (1998). "Positive streamer propagation in large oil gaps: Experimental Characterization of Propagation Modes", IEEE Trans. Dielectrics Electr. Insul. (3):360-370.

Linhjell D, Lundgaard L, Berg G (1994). "Streamer propagation under impulse voltage in long point-plane oil gaps", IEEE Trans. Dielectrics Electr. Insul. I(3):447-458.

Liu Q, Wang Z, Perrot F (2009). "Impulse breakdown voltages of ester-based transformer oils determined by using different test methods," in IEEE Conf. Electr. Insul. Dielectric Phenomena, CEIDP'09, IEEE, 2009, pp. 608–612.

Lopatin V, Noskov MD, Badent R, Kist K, Schwab AJ (1998). "Positive discharge development in insulating oil: optical observation and simulation", IEEE Trans. Dielectrics Electr. Insul. 5(2):250-255.

Martin D, Wang Z (2008). "Statistical analysis of the ac breakdown voltages of ester based transformer oils," IEEE Trans. Dielectrics Elect. Insul. 15(4):1044–1050.

Martin MAG (2010). "Vegetable oils, and alternative to mineral oil for power transformers", IEEE Electrical Insulation Magazine, 26(6):7-13.

Massala G, Lesaint O (2001). "A comparison of negative and positive streamers in mineral oil at large gaps", J. Phys. D: Appl. Phys. 34(10):1525-1532.
McShane C, Corkran J, Harthun R, Gauger G, Rapp K, Howells E (2000). “Vegetable oil based dielectric coolant,” Mar. 14 2000, US Patent 6,037,537.
McShane CP, Gauger GA, Luksich J (1999). “Fire Resistant Natural Ester Dielectric Fluid and Novel Insulation System for its Use. Proc. of IEEE/PES Transmission and Distribution Conference, 1999.
Moumine I, Gosse B, Gosse J, Clavreul R, Hantouche C (1995). “Vegetable oil as an impregnant in hv ac capacitors,” in IEEE 5th Int. Conf. Conduction Breakdown Solid Dielectrics, ICSD’95, 1995, pp. 611–615.
Nelson J (1980). “Insulating liquids: Their uses, manufacture and properties,” Electronics Power 26(6):481.
Oommen T (2002). “Vegetable oils for liquid-filled transformers,” IEEE Electrical Insul. Magazine, 18(1):6–11.
Oommen T, Claiborne C (1999). “Electrical transformers containing electrical insulation fluids comprising high oleic acid oil compositions,” Sep. 7 1999, US Patent 5,949,017.
Perrier C, Beroual A, Bessede J (2004). “Experimental investigations on different insulating liquids and mixtures for power transformers,” in Conference Record of the IEEE Int. Symposium Electrical Insul. pp. 237–240.
Rapp K, Corkran J, Mcshane C, Prevost T (2009). “Lightning impulse testing of natural ester fluid gaps and insulation interfaces,” IEEE Trans. Dielectrics Elect. Insul. 16(6):1595–1603.
Sharbaugh A, Devins J, Rzad S (1978). “Progress in the field of electric breakdown in dielectric liquids,” IEEE Trans. Elect. Insul. 4:249–276.
Stockton DP, Bland JR, McClanahan T, Wilson J, Harris DL, McShane P (2007). "Natural Ester Transformer Fluids: Safety, Reliability & Environmental Performance," Petroleum and Chemical Industry Technical Conf. (PCIC '07): 1-7.
Torshin YV (2003). "Prediction of Breakdown Voltage of Transformer Oil from Predischarge Phenomena", IEEE Trans. Dielectrics Electr. Insul. 10(6):933-941.
Torshin YV (2009). "Initiation and propagation of the negative leader in transformer oil under impulse voltage", IEEE Trans. Dielectrics Electr. Insul. 16:1536-1542.
Viet-Hung D, Beroual A, Perrier C (2012). “Investigation on streamers phenomena in mineral, synthetic and natural ester oils under lightning impulse voltage”, IEEE Trans. DEI. 19(5):1521-1527.
Yasuda K, Arazoe S, Igarashi T, Yanabu S, Ueta G, Okabe S (2010). “Comparison of the insulation characteristics of environmentally-friendly oils,” IEEE Trans. Dielectrics Elect. Insul. 17(3):791–798.

academicJournals

Vol. Vol. 9(13), pp. 302-308, 16 July, 2014
DOI: 10.5897/IJPS2014.4157
ISSN 1992 - 1950
Article Number: 9BE0C0946337

http://www.academicjournals.org/IJPS

International Journal of Physical Sciences

Full Length Research Paper

An efficient technique for morphing zero-genus 3D objects

A. Elef, M. H. Mousa* and H. Nassar

Department of Computer Science, Faculty of Computers and Informatics, Suez Canal University, Egypt.

Received 30 April, 2014; Accepted 10 July, 2014

In this paper, we present an algorithm to morph a zero-genus mesh model to a topologically equivalent one based on spherical parameterization, as it is the natural parameterization method for this kind of objects. Our algorithm starts by normalizing the two objects to the cube of unity, as a preprocessing step. Then, the two normalized models are parameterized onto a common spherical domain. We reposition the points of the objects on the sphere in accordance to the relative areas of their triangles. Repositioning on the sphere prevents point clustering and overlapping during the matching process. Experimental results are presented to demonstrate the efficiency of the algorithm.

Key words: 3D morphing, zero-genus mesh, spherical parameterization, nearest neighbor matching.

INTRODUCTION

Shape changing has gained attention due to the attraction of scenes people see on the screen. Indeed, morphing is derived from the biological term “metamorphosis”, meaning the change in form and often habits of the individual during normal development after the embryonic stage. Therefore, it suits very well modeling computer animation techniques dealing with the design of algorithms changing one object into another over time (Sompagdee, 2009). In other terms, morphing is an interpolation technique used to create from two objects a series of intermediate objects that change continuously to make a smooth transition from the source object to the target object. Morphing has been done in two dimensions by varying the values of the pixels of one image to make a different image, or in three dimensions by doing the same. We are presenting here a new type of morphing, which is applied to the geometry of three dimensional models, creating intermediate 3D objects which can be translated, rotated, scaled, and zoomed into.

The history of morphing can be categorized into two categories: 2D and 3D morphing. 2D morphing seems to have reached its goals in finding the solutions for the transformations as well as feature handling, while 3D morphing is still far behind 2D success (Sompagdee, 2009).

Two-dimensional morphing

In general, 2D morphing techniques require a lot of manual processes. They can be classified into two categories: image-based and geometric-based.

*Corresponding author. E-mail: amira_mohamed@ci.suez.edu.eg, mohamed_mousa@ci.suez.edu.eg, nassar@ci.suez.edu.eg

Image-based morphing

Image-based approaches are used enormously in the entertainment industry. Algorithms here are generally composed of three major steps: control, warping and cross dissolving. For controlling the morphing process, these algorithms rely heavily on the experience and knowledge of animators to define correspondence points. Good results can be obtained by using images captured from similar angles and positions regarding the lack of the depth information for generating intermediate objects. Beier and Neely (1992) proposed the line segment feature based method. Where, animators have less work but the complexity of calculation is increased. Lee et al. (1995) used moving curves called snakes in order to capture features accurately and fasten the process of feature defining.

Geometric-based morphing

For geometric–based approaches, 2D polygons are given as input. Sederberg and Greenwood (1992) proposed a minimization method without user interaction. New vertices are added to the polygon that has less number of vertices. All possible paths are calculated but only the best path, the one that gives a minimum amount of work or less shrinkage, is selected. Gao and Sederberg (1998) improved the method to measure the amount of work as well as the way to find the least work path. Shapira and Rappoport (1995) embedded skeletons inside each polygon by decomposing the polygon into star-shaped pieces with a star origin inside each piece then they connected those star origins. For interpolation, skeletons are interpolated and star pieces are unfolded.

Three-dimensional morphing

Three- dimensional morphing algorithms transform a 3D model into another. The complexity of an algorithm depends on many factors, such as: the object representation, genus, and convexity. The simplest morphing can be done when the initial and final shapes are convex and similar in their geometry and topology. Usually, 3D methods have restrictions on object models and how models are represented. Concave objects are more difficult to morph than convex ones. Objects with a different genus, e.g. with holes or with a closed surface are very complicated to transform. Without user intervention, it is not possible to get the desirable results. The existing solutions are categorized by object representations as follow (Sompagdee, 2009):

(i) Polygonal-based representation: The objects are represented by their boundaries. This representation is commonly used and is easy to obtain.

(ii) Volumetric representation: The 3D models are described either by their geometric primitives or by volumes (volumetric data sets). A volumetric representation is ideal for modeling the behavior of objects with complex interior structures. In particular, this representation helps overcome the limitation on model types.

CONTRIBUTION

Our approach is focused on creating the series of intermediate objects, using spherical parameterization as a common domain of the source and target zero-genus objects. This parameterization domain is the natural domain to use, given when our object is a sphere, and as such- makes the mapping step easier.

To create this series of intermediate objects, we start by parameterizing the source and target objects on the sphere. We use progressive meshes (Hoppe, 1996; Zhou et al., 2004) in combination with a local smoothing strategy (Shen and Makedon, 2006) to find the final spherical parameterization. Then we create the point-to-point correspondence between the objects using the AABB tree search technique (CGAL, 2010). The spherical parameterization which we have used makes the mapping step easier since the objects are mapped to their natural parameterization domain.

Initial spherical parameterization

Parameterization of 3D mesh data is important in such applications as, texture mapping, remeshing and morphing. Closed manifold genus-0 meshes are topologically equivalent to a sphere; hence this is regarded as the natural parameterization domain for it. Parameterizing a triangle mesh onto a sphere means assigning a 3D position on the unit sphere to each of the mesh vertices, such that the spherical triangles induced by the mesh connectivity are not too distorted and do not overlap. Satisfying the non-overlapping requirement is the most difficult and critical component of this process. Moreover, it is usually an expensive optimization procedure for large meshes. Here, we describe the spherical parameterization algorithm we use, which is based on the algorithm proposed in (Praun and Hoppe, 2003; Zhou et al., 2004; Shen and Makedon, 2006). The later algorithm incorporates a local parameterization scheme into the progressive mesh representation (Hoppe, 1996). This reduces the complexity of global optimization for large meshes.

Given a triangle mesh M, the problem of spherical parameterization is to form a continuous invertible mapψ from the unit sphere to the mesh. That's, $\psi: S^2 \rightarrow M$. The map is specified by assigning for each mesh vertex v a parameterization $\psi^{-1}(v) \in S^2$. Therefore, each mesh

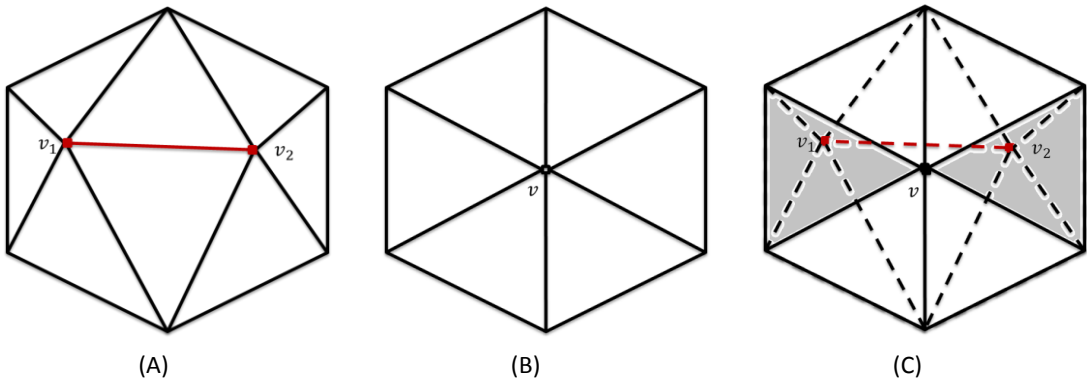

Figure 1. An edge collapse operation. (A) (Left) the edge v to be collapsed. (B) (Middle) The mesh after the edge contraction. (C) (Right) Parameterizing the deleted vertices using the created triangles.

edge is mapped to a great circle arc, and each mesh triangle is mapped to a spherical triangle bounded by these arcs. The spherical parameterization algorithm consists of two major steps:

(i) A progressive mesh representation, $\mathcal{M} = \{M^0, M^1, \cdots, M^k = M\}$, with embedded local parameterization information is generated from the original mesh M. This is performed by iterating the successive edge collapse operations until the current simplified mesh becomes a convex polyhedron M^0. The obtained polyhedron is considered as the base mesh of $\mathcal{M}$. For each edge collapse, the two decimated vertices are parameterized over the resulting simplified mesh. The local parameterization information is recorded in $\mathcal{M}$.
(ii) Suppose that the centroid of the base mesh M^0 is the center of the unit sphere. The projection of the vertices of M^0 onto the considered sphere produces an initial spherical mesh. Starting from this initial spherical mesh, the sequence of vertex split operations, the inverse of the edge collapse, in $\mathcal{M}$ is performed progressively. For each vertex split operation, the two split vertices are positioned on the unit sphere using the recorded connectivity and embedded parameterization information.

The key point of the progressive mesh hierarchical structure is the choice of the order of the edges to be collapsed. Here, we use the selection strategy proposed by Garland and Heckbert (1997) to determine the edge collapse order and to position the newly created vertices. In the classical progressive mesh representation (Hoppe, 1996; Zhou et al., 2004), the geometrical and topological information of each removed vertex are recorded in a vertex splitting operation during the decimation process. Thus the vertex can be completely recovered during progressive refinement process. However, this information is not suitable to reposition the recovered vertex on the unit sphere when the same vertex split sequence is performed on the corresponding spherical mesh. In what follows, we present how to reposition the recovered vertex according to the relative position with respect to its first order neighborhood in the original mesh. As shown in Figure 1 (left and middle), edge $e = v_1v_2$ is collapsed and a new vertex v is created. Let $star(v)$ be first order neighborhood of the vertex v. Using the MAPS algorithm (Lee et al., 1998), $star(v)$ is flattened into a planar region Ω. The vertices v_1 and v_2 are embedded into Ω and find the triangles T_1 and T_2 containing v_1 and v_2 respectively. The barycentric coordinates $(\alpha_i, \beta_i, \gamma_i)$, $i = 1,2$ of the embedding of v_1 and v_2 inside T_1 and T_2 respectively. Therefore, v_1 and v_2 can be locally parameterized with respect to the containing triangles T_1 and T_2 using the barycentric coordinates $(\alpha_i, \beta_i, \gamma_i)$. The local parameterization information of the two decimated vertices, together with all collapse information of the edge, is recorded in a vertex split operation for later reconstruction on the sphere. The final form of the progressive hierarchy of the given mesh is $\mathcal{M} = \{M^0, sp^1, sp^2, \cdots, sp^k\}$, where M^0 is the convex base mesh and the sp^i are the ordered split operations. That is, $M^i = M^0, sp^1, \cdots, sp^i$.

Starting from this base spherical mesh which is generated by projecting the convex base mesh M^0 onto the unit sphere, the vertex split operations in $\{sp^1, sp^2, \cdots, sp^k\}$ are performed progressively to simultaneously recover the original mesh and construct the spherical parameterization. Let M^i be the recovered mesh after performing the $i$ths vertex split operation, M_s^i be its corresponding spherical mesh. The $(i+1)$ths vertex split operation is then performed as follows. With the containing triangles T_1, T_2 and barycentric coordinates $(\alpha_i, \beta_i, \gamma_i)$ of the two new vertices v_1' and v_2' retrieved from sp^{i+1}; two new vertices v_1' and v_2' are inserted into M_s^{i+1} with the same connectivity as in M^{i+1} and positioned on the unit sphere by:

$$v_1' = Normalize(\alpha_1 p_1^1 + \beta_1 p_1^2 + \gamma_1 p_1^3)$$
$$v_2' = Normalize(\alpha_2 p_2^1 + \beta_2 p_2^2 + \gamma_2 p_2^3)$$

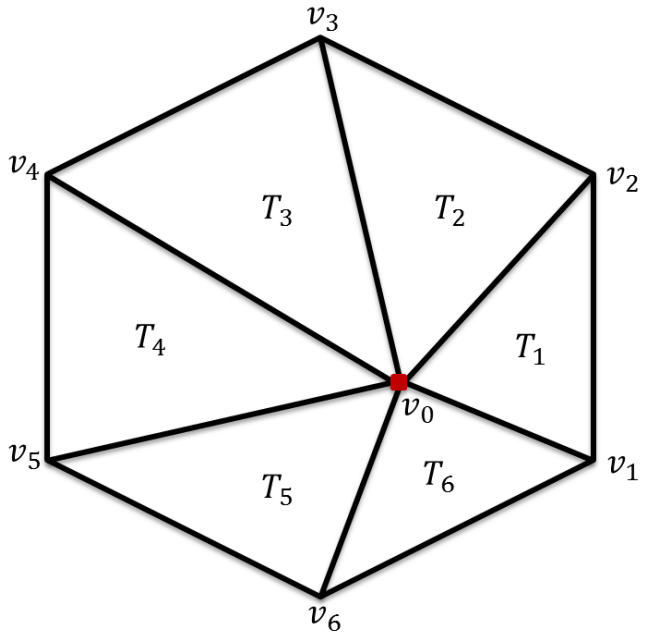

Figure 2. The local neighborhood $star$ projected on the 2D plane.

Where (p_1^1, p_1^2, p_1^3) and (p_2^1, p_2^2, p_2^3) are the triangles in M_s^i corresponding to T_1 and T_2 respectively.

Local spherical improvement

The local spherical improvement uses iterations overthe vertices of the initial parameterization on the unit sphere (Shen and Makedon, 2006). At each vertex, it tries to reposition in the local neighborhood $star$ to gradually improve the mapping quality. The triangles composing the local neighborhood $star$ is piece-wise linear. Therefore it can be projected on the 2D plane while preserving the relative area of each spherical triangle. Given that the vertex to reposition, Figure 2 shows an example of the projection of $star$ on a 2D plane. Supposing that $v_i = (x_i$, the signed area of the triangle can be computed by:

$$A_1 = \frac{1}{2}\left((x_2 - x_1)(y_0 - y_1) - (x_0 - x_1)(y_2 - y_1)\right)$$

Thus, replacing A_1 with A_{ideal} and treating $x_0$and y_0 as the only unknowns in the previous equation, we can formulate a system of linear equations using all the triangles in the spherical$star(v_0)$and solve it in the least squares sense to locate a new center vertex position. This new center position minimizes the square sum of the relative area differences between $star(v_0)$ on the object and $star(v_0)$ on the sphere S^2. Note that only the center position is concerned here. This indicates that the border of spherical $star(v_0)$is fixed,and consequently that. the total area of the spherical $star(v_0)$cannot be changed. Therefore, each triangle in the spherical $star(v_0)$ aims to achieve not its correct absolute area but the correct area relative to the other triangles in $star(v_0)$. For example, Let$T_1, T_2, \cdots, T_6$ be the set of projected triangles depicted in Figure 2 and $T_1', T_2', \cdots, T_6'$ be the corresponding triangles on the object. If we use $A(\cdot)$ to denote the area of a triangle, the relative area of T_i' can be given by:

$$T_i = \frac{A(T_i')}{\sum_{j=1}^{6} A(T_j')}$$

In order to preserve this relative area, on the 2D project should have an ideal area of,

$$A_i = \frac{A(T_i')}{\sum_{k=1}^{6} A(T_k')} A_{Total}$$

Where A_T, is the total area of the 2D projection of the parameter submesh. To calculate the new location (x) for the parameter submesh center on its 2D projection, the following system of linear equations is formulated:

$$\begin{aligned}
(x_2 - x_1)(y - y_1) - (x - x_1)(y_2 - y_1) &= 2A_1 \\
(x_3 - x_2)(y - y_2) - (x - x_2)(y_3 - y_2) &= 2A_2 \\
(x_4 - x_3)(y - y_3) - (x - x_3)(y_4 - y_3) &= 2A_3 \\
(x_5 - x_4)(y - y_4) - (x - x_4)(y_5 - y_4) &= 2A_4 \\
(x_6 - x_5)(y - y_5) - (x - x_5)(y_6 - y_5) &= 2A_5 \\
(x_1 - x_6)(y - y_6) - (x - x_6)(y_1 - y_6) &= 2A_6
\end{aligned}$$

The new center location $(x$ is obtained by solving this linear system in a least squares sense.

MESH MAPPING

Now that we have the source and the target 3D objects parameterized on the sphere, the objective here is to find the point-to-point correspondence between the two parameterized objects. According to the number of points in the two objects, we have two kinds of mesh mapping:

(i) M to M mapping: The two input objects have the same number of points. We use the nearest neighbor algorithm (Manolis et al., 1997) to find the point to point correspondence. To avoid the case that multiple points are matched to a single point, we associate with each point an attribute, valued by true or false, to indicate whether that point is selected before or not.

(ii) M to N mapping: The source and the target objects have not the same number of points. Without loss of generality, assume that the source object has more points than the target object. To overcome this inequality problem we subdivide the target object using the subdivision algorithm (Kobbelt, 2000) such that the two

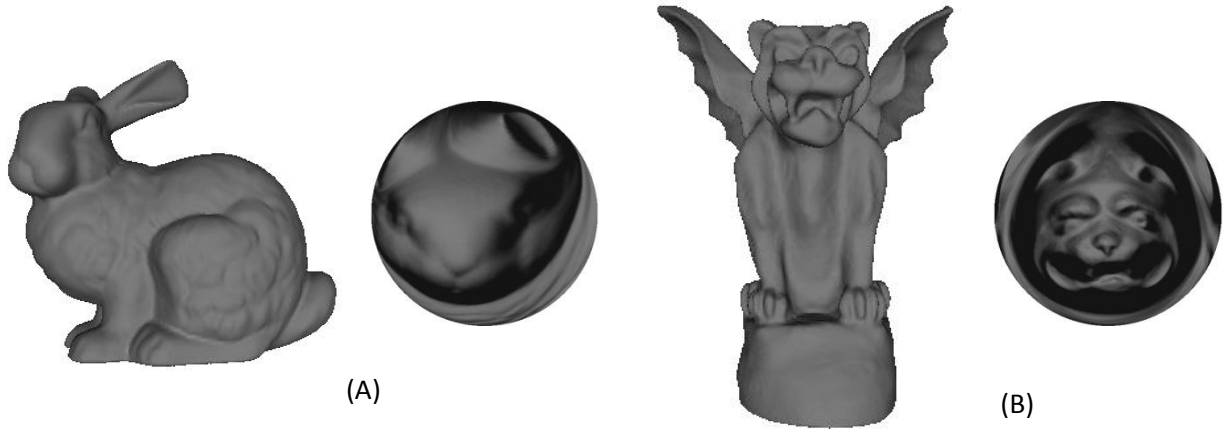

Figure 3. (A) Left two images. The input triangular mesh of the Stanford Bunny (39 k points, 70 k triangles) and, its spherical parameterization, (B) Right two images. The target triangular mesh of the Gargoyle (100 k points and 200 k triangles) and its spherical parameterization.

objects have an equal number of points. We fall again in the first kind-- M to M mapping. It can be seen that M to N mapping is more costly than M to M mapping, simply since we apply M to M mapping in addition to the subdivision step.

M to N mapping has the disadvantage of being time consuming. We use an enhanced implementation of nearest neighbor searching called AABB tree (CGAL, 2010). The AABB tree features a static data structure and algorithms to perform efficient intersection and distance queries against sets of finite 3D geometric objects. Using this static data structure, we build a tree with the vertices of the target object. We then use the tree to find for each point of the source object the corresponding nearest neighbor from the tree.

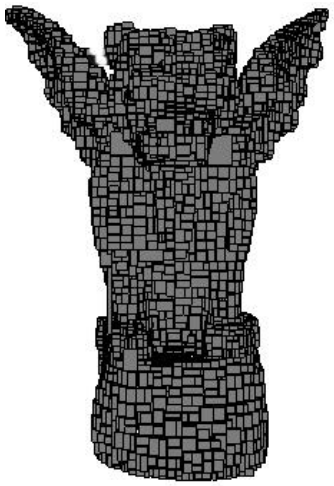

Figure 4. The AABB tree for the set of the spherical triangles of the gargoyle.

RESULTS

The methods described in the preceding sections have been implemented in C++ and using CGAL the Computational Geometry Algorithms Library (CGAL, 2010). The experiments are carried out on a PC with a 2.8 GHZ dual-core processor and 2GB of memory. The input objects are in the form of triangular meshes. Before constructing the spherical parameterization of our objects, we apply the following two preprocessing steps:

(1) Normalize the input models to a cube of unityto get a smooth and a robust transition between the input and output objects. This normalization of each object is performed separately. For each object, the centroid of the object is translated to the origin of the coordinates. Then, calculate the distance, of the farthest point with respect to the origin. Finally, divide the coordinates of each point, $p = (p_x, p_y, p_z)$, by d to get the normalized point $p_{Norm} = \left(\frac{p_x}{d}, \frac{p_y}{d}, \frac{p_z}{d}\right)$.

(2) If the objects are not sufficiently sampled, apply surface subdivision to enhance the mapping between the input and output objects.

Figure 3 shows the spherical parameterization of two triangular meshes the input object is the Stanford bunny and the target object is the Gargoyle. In our experiment, the parameterization time is 79 s for the Gargoyle (100 k points and 200 k triangles). Once the spherical parameterization is constructed for the input and target objects, we construct the AABB tree for the set of spherical triangles of the target object (the gargoyle, in our case) for the mapping step, as shown in Figure 4.

Figure 5. The sequence of morphing the stanford bunny to the gargoyle.

Each point in the spherical parameterization of the Bunny is matched with the closest spherical point in the AABB tree.

Once the matching step is performed, a linear interpolation is performed between the set of points of the Bunny and the corresponding points in the Gargoyle. This interpolation creates the set of frames to be visualized as the final morphing animation. Figure 5 shows the series of the frames that creates the morphing of Bunny-Gargoyle.

CONCLUSIONS

In this paper, we propose a novel technique for 3D mesh morphing capable to interpolate between arbitrary zero-genus objects. The technique can be presented as an animation by creating a series of intermediate objects using the spherical parameterization as a common domain of the source and target objects. We converted both objects into the same spherical domain with suitable modifications to reposition of the points on the sphere. This repositioning prevents the morphing from creating overlapping or clustering of points on the sphere during the mapping step.Then we carry out mesh mapping to realize the morphing process and this happened by using the point-to-point correspondence between the objects of the AABB tree search algorithm. The spherical parameterization which is used to make the mapping step easy since the objects are mapped to their natural parameterization domain.

Conflict of Interest

The author(s) have not declared any conflict of interest.

REFERENCES

Beier T, Neely S (1992). Feature-Based Image Metamorphosis. Proceedings of SIGGRAPH 92:35-42.

CGAL (2010). Computational Geometry Algorithms Library, http://www.cgal.org.

Garland M, Heckbert PS (1997). Surface simplification using quadric error metrics. Proceedings of the 24th annual conference on Computer graphics and interactive techniques, ACM Press/Addison-Wesley Publishing Co. 209-216.

Gao P, Sederberg TW (1998). “A Work Minimization Approach to Image Morphing,” Visual Computer, pp. 390-400.

Hoppe H (1996). Progressive meshes. Proceedings of the 23rd annual conference on Computer graphics and interactive techniques, ACM. pp. 99-108.

Kobbelt L (2000). sqrt(3)-subdivision. Computer Graphics (Proc. SIGGRAPH '00). 34:103-112.

Lee AWF, Sweldens W, Schroder P, Cowsar L, Dobkin D (1998). MAPS: multiresolution adaptive parameterization of surfaces. Proceedings of the 25th annual conference on Computer graphics and interactive techniques, ACM: pp. 95-104.

Lee S, Chwa K, Shin SY, Wolberg G (1995). “Image Metamorphosis Using Snakes and Free-form Deformations. Proceedings of SIGGRAPH 95.

Manolis K, Hoomanvassef MDB, Krzysztof G (1997). "3D MOrphing." MIT project (6.837) http://web.mit.edu/manoli/morph/www/morph.html.

Praun E, Hoppe H (2003). "Spherical parametrization and remeshing." ACM. Trans. Graph. 22(3):340-349.

Sederberg TW, GreenWood E (1992). A Physically Based Approach to 2D Shape Blending. Proceedings of SIGGRAPH 92. In Computer Graphics Proceedings, Annual Conferences Series.

Shapira M, Rappoport AA (1995). "Shape Blending Using Star-Skeleton Representation." IEEE Computer Graphics and Applications. pp. 44-50.
Shen L, Makedon F (2006). "Spherical mapping for processing of 3D closed surfaces." Image Vision Computing. 24(7):743-761.
Sompagdee P (2009). Survey of Morphing. C. S. Department, Thammasat University. pp.1-8.
Zhou K, Bao H, Shi J (2004). "3D surface filtering using spherical harmonics." Computer-Aided Design. 36(4):363-375.

International Journal of Physical Sciences

Related Journals Published by Academic Journals

- *African Journal of Pure and Applied Chemistry*
- *Journal of Internet and Information Systems*
- *Journal of Geology and Mining Research*
- *Journal of Oceanography and Marine Science*
- *Journal of Environmental Chemistry and Ecotoxicology*
- *Journal of Petroleum Technology and Alternative Fuels*

academicJournals